

Hard X-ray variability of V404 Cyg during the 2015 outburst[★]

C. Sánchez-Fernández¹, J. J. E. Kajava¹, S. E. Motta², and E. Kuulkers¹

¹ European Space Astronomy Centre (ESA/ESAC), Science Operations Department, E-28691, Villanueva de la Cañada, Madrid, Spain
e-mail: Celia.Sanchez@sciops.esa.int

² University of Oxford, Department of Physics, Astrophysics, Denys Wilkinson Building, Keble Road, Oxford OX1 3RH, UK

Received August, 2016; accepted ..., ...

ABSTRACT

Aims. Hard X-ray spectra of black hole binaries (BHB) are produced by Comptonization of soft seed photons by hot electrons near the black hole. The slope of the resulting energy spectra is governed by two main parameters: the electron temperature and the optical depth of the emitting plasma. Given the extreme brightness of V404 Cyg during the 2015 outburst, we aim to constraint the source spectral properties using an unprecedented time resolution in hard X-rays, and to monitor their evolution over the whole outburst.

Methods. We have extracted and analyzed 602 X-ray spectra of V404 Cyg obtained during the 2015 June outburst by the IBIS/ISGRI instrument onboard *INTEGRAL*. We have performed time-resolved spectral analysis, using a time resolution ranging between 64 and 176000 seconds. The spectra were fitted in the 20–200 keV energy range.

Results. We find that while the V404 Cyg light curve and soft X-ray spectra are remarkably different from other BHBs light curves, the spectral evolution of V404 Cyg in hard X-rays and the relations between the spectral parameters are consistent with those observed in other BHBs. We identify a *hard branch* where the electron temperature is anti-correlated with the hard X-ray flux, and a *soft flaring branch* where the relation reverses. In addition, we find that during the long X-ray plateaus detected at intermediate fluxes, the thermal Comptonization models fail to describe the spectra.

Conclusions. We conclude that the *hard branch* in V404 Cyg is analogous to the canonical hard state of BHBs. V404 Cyg never seems to enter the canonical soft state, although the soft flaring branch bears resemblance to the BHB intermediate state and very high state. The X-ray plateaus are likely produced by absorption in a Compton-thick outflow, where the extreme absorption columns reduce the observed flux by a factor of about 10. Variable covering fractions of the central source may be the reason for the complicated light curve variability, rather than intrinsic source variability.

Key words. Accretion, accretion disks – Black hole physics – X-rays: binaries – X-rays: individuals: V404 Cyg

1. Introduction

Black hole (BH) binary systems (BHBs) can go through various spectral states which are thought to be caused by changes in the accretion geometry and accretion rates close to the BH, although the actual details of still remain debated (Remillard & McClintock 2006; Belloni & Motta 2016). The two most common states are the *hard* and the *soft* states (see, e.g., Done et al. 2007; Poutanen & Veledina 2014 for review). In the *hard state*, the spectrum can be described by a power-law with a variable cutoff around 60–150 keV, which is thought to result from Comptonization of soft seed photons by a population of hot electrons located in an optically thin region close to the BH (Shapiro et al. 1976; Narayan & Yi 1995). The high energy cut-off suggests a thermal distribution of electrons, with temperatures in the range 30–100 keV (Sunyaev & Truemper 1979; Gierliński et al. 1999). Occasionally, a hard excess has been observed above 100 keV suggesting the presence of non-thermal electrons as well (see e.g., McConnell et al. 2002; Wardziński et al. 2002; Joinet et al. 2007; Droulans et al. 2010),

either in the corona/hot flow or in the base of the jet (e.g., Zdziarski et al. 2012).

In the *soft state*, thermal emission peaking at ~ 1 keV, from a cool, optically thick, geometrically thin accretion disk, dominates the spectrum (Shakura & Sunyaev 1973; Esin et al. 1997). A weak, hard X-ray tail extending up to the MeV range, is also detected (Zdziarski et al. 2016). This tail is thought to originate from Comptonized emission by non-thermal electrons in discrete flares on top of the accretion disc (McConnell et al. 2002). During transitions between the hard and soft states, BHBs pass through additional *intermediate* states, which show characteristic features of both (see e.g. Ebisawa et al. 1994; Malzac et al. 2006; Belloni & Motta 2016). On rare occasions, some systems may pass also through the so-called *very high state* (also called *ultra-luminous* or *anomalous* state, e.g., Motta et al. 2012), an intermediate state characterized by both a strong thermal component and a very strong and steep hard X-ray tail (Done et al. 2007; Motta et al. 2012).

One of the current observational challenges in this context is to determine the electron temperature, T_e , and optical depth, τ , of the Comptonizing medium. These together determine the spectral slope of the Comptonized spectrum (e. g. Beloborodov 1999). Because the cutoff are found around 100 keV, where usually the instrumental response is low, observations sensitive enough to constrain these parameters have been only available

[★] Based on observations with INTEGRAL, an ESA project with instruments and science data centre funded by ESA member states (especially the PI countries: Denmark, France, Germany, Italy, Switzerland, Spain) and with the participation of Russia and the USA.

for a few sources and typically require long exposures. Observations in the *hard state* of GRO J0422+32 (Esin et al. 1998), GX 339–4 (Wardziński et al. 2002; Motta et al. 2009), XTE J1550–564 (Rodríguez et al. 2003), Cyg X-1 (Del Santo et al. 2013) and Swift J1753.5–0127 (Kajava et al. 2016) show anti-correlation between electron temperature, T_e (or high energy cut-off) and X-ray flux, accompanied by an increase in the plasma optical depth as the flux increases (Wardziński et al. 2002). The relation reverses during the *hard* to *soft* state transitions. Observations of these transitions in Cyg X-1 (Phlips et al. 1996; Del Santo et al. 2013), GRO J1719–24 (Esin et al. 1998), GRO J1655–40 (Joinet et al. 2008) and GX 339–4 (Motta et al. 2009) show an increasing T_e with increasing flux, while the optical depth τ decreases (Joinet et al. 2008; Del Santo et al. 2013). The cutoff is significantly present during the hard and intermediate states, and it disappears when the source reaches the soft state.

The extremely bright outburst of V404 Cyg in June 2015, provides a unique data set to perform time resolved spectroscopy and study in detail the evolution of the parameters describing the Comptonizing plasma. We present here the results of IBIS/ISGRI spectral analysis in the 20–200 keV energy range over the period 18–28 June 2015.

V404 Cyg is a transient Low-Mass X-ray binary (LMXB) consisting of a $9.0^{+0.2}_{-0.6} M_\odot$ BH accreting mass from a K3 III companion (Khargharia et al. 2010) in a 6.5 d orbit (Casares et al. 1992). It is located at a distance $d = 2.39 \pm 0.14$ kpc (Miller-Jones et al. 2009). V404 Cyg was first detected in optical wavelengths during two outbursts in 1938 and 1956 (Richter 1989) and later in X-rays during a third outburst in 1989 (Makino 1989; Marsden 1989), characterized by extreme flaring activity, several flux levels above the Crab (Tanaka 1989; Oosterbroek et al. 1996). After ~ 26 years in quiescence, the onset of a new outburst was detected by *Swift*/BAT and MAXI and *Fermi*/GBM on 15 June 2015 (Barthelmy & Sbarufatti 2015; Negoro et al. 2015; Younes 2015). This outburst, which triggered the most intensive multi-wavelength observing campaign performed so far on a transient BHB, lasted until early-August 2015 (Sivakoff et al. 2015). During the first ten days, the source exhibited violent flaring activity on time scales of sub-seconds to hours in all the observed wavelengths: γ -rays (Loh et al. 2016); X-rays (Rodríguez et al. 2015; Roques et al. 2015; Jenke et al. 2016; Walton et al. 2016); Optical (Gandhi et al. 2016; Kimura et al. 2016; Muñoz-Darias et al. 2016); Infrared (Eikenberry et al. 2016); Millimeter/Sub-millimeter and Radio (Tetarenko et al. 2015). In some major flares, V404 Cyg reached fluxes around 50 and 40 Crab in soft and hard X-rays respectively (Segreto et al. 2015; Rodríguez et al. 2015). The peak of the outburst was reached on June 26th, and the flux dropped immediately afterwards (Ferrigno et al. 2015; Walton et al. 2015) slowly fading to quiescence over the subsequent weeks (Sivakoff et al. 2015).

2. Observations and data analysis

V404 Cyg was observed by *INTEGRAL*, the INTErnational Gamma-Ray Astrophysics Laboratory (Winkler et al. 2003) in a series of Target of Opportunity observations scheduled between 17 June, 2015 and 13 July, 2015 (revolutions 1554–1563; Kuulkers 2015). We present here the analysis of the available IBIS/ISGRI data (Lebrun et al. 2003), obtained during revolutions 1554–1558 (18–28 June, 2015; MJD 57191–51201), which cover the epoch of intense flaring activity and the beginning of the outburst decay (see Fig. 1a). These observations provide data

sensitive enough to study in detail the properties of the Comptonizing medium.

2.1. Data reduction

The IBIS/ISGRI data reduction was performed using the Off-line Scientific Analysis software (OSA; Courvoisier et al. 2003) v10.2, using the latest calibration files. The data were processed following standard IBIS/ISGRI reduction procedures.

The spectral extraction was performed using good time interval files (GTIs) of variable duration, defined to provide source spectra of comparable S/N regardless of the source flux. The GTI selection was based on the source light curves distributed by the INTEGRAL Science Data Center (ISDC; Kuulkers 2015). We extracted 602 IBIS/ISGRI spectra, with exposure in the range 64 to 176000 s. We binned the IBIS/ISGRI response matrix in the energy range 20–500 keV using 28 channels of variable logarithmic widths. In order to remove potential background contamination, and the contribution of intrinsic spectral components above 200 keV, like hard non-thermal tails (Rodríguez et al. 2015; Roques et al. 2015) or hard X-ray emission caused by positron annihilation (Siegert et al. 2016), we restricted the spectral fits to the 20–200 keV energy range. In our fits we have ignored the energy bin around 50 keV and added 3 per cent systematic errors to the spectral bins. The IBIS/ISGRI X-ray spectra were fit using *XSPEC* v12.8.2, adopting the χ^2 statistics. Errors provided below are quoted at the 1- σ confidence level ($\Delta\chi^2 = 1$ for one parameter of interest).

2.2. Spectral modelling

In Fig. 2 we provide a sample of the V404 Cyg IBIS/ISGRI spectra analysed in this work. In most occasions the spectrum displays a powerlaw-like shape, modified by a cut-off at high energies, consistent with the effects of thermal Comptonization (see Fig. 2a). Therefore, we have applied Comptonization models to fit our data: *NTHCOMP* (Zdziarski et al. 1996; Życki et al. 1999) and *COMPBS* (Poutanen & Svensson 1996). These models provide a description of the continuum produced by thermal Compton up-scattering of soft X-ray photons. *NTHCOMP* is parameterized by a power law index Γ , and an electron temperature T_e . The *COMPBS* parameters are the electron temperature T_e and optical depth τ . In both models we fixed the seed photon temperature, T_{bb} to 0.1 keV, as it could not be constrained even by the *Swift*/XRT data (Motta et al. 2016, in preparation). Although Natalucci et al. (2015), Roques et al. (2015) and Jenke et al. (2016) inferred seed photon temperatures ~ 6 –7 keV, we regard it likely that these values are due to unmodelled absorption. Very strong absorption ($N_H \gtrsim 10^{24} \text{ cm}^{-2}$) imposes a curvature in the observed spectrum towards lower energies, which likely lead to high inferred T_{bb} values.

In some cases, a high-energy cutoff is either weakly significant or not statistically required by the data (see figure 2b). These spectra can still be fit using Comptonization models, but fixing T_e to an arbitrary high value ($T_e = 999$ keV). To account for both possibilities, we have carried out two independent fitting runs per model: in the first fitting run, we left the electron temperature, T_e , as a free parameter, while in the second fitting run we fixed it to $T_e = 999$ keV. Then, the Bayesian information criterion (BIC; Schwarz 1978) has been applied to the results derived for each spectrum in order to determine the best fit to the data. We computed the BIC using the following approximation: $\text{BIC} = \chi^2 + k \ln(n)$, where k is the number of parameters in the

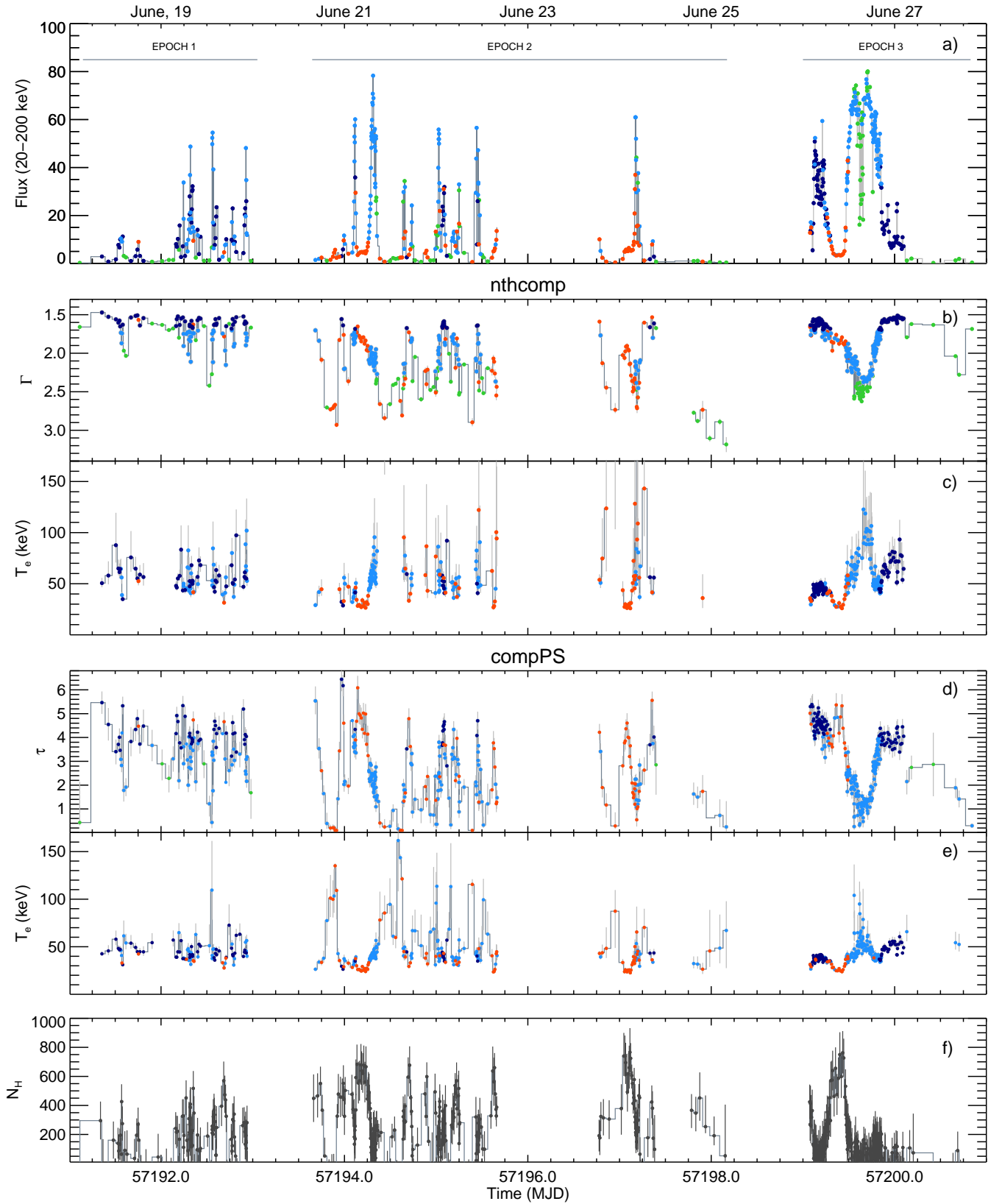


Fig. 1. Time evolution of the flux and spectral parameters of V404 Cyg observed during the June 2015 flaring episodes. **Panel a)** source flux (20–200 keV) in units of $10^{-8} \text{ erg cm}^{-2} \text{ s}^{-1}$. **Panel b, c)** nTHCOMP fitting parameters (power-law index, Γ , and electron temperature, T_e). **Panel d, e)** compPS fitting parameters (optical depth, τ , and electron temperature, T_e). **Panel f)** N_H ($\times 10^{22} \text{ cm}^{-2}$) values derived adding an absorption component TBABS to our spectral fits. Note, however that in panels a–e, N_H is not considered, as it is not well constrained by our spectral fits in all cases. Green, blue and red symbols are used to highlight the best-fitting model, according to our model selection criteria (Sect. 2.2). Blue: Comptonization models with constrained T_e (Fig. 2a) further divided into hard ($\Gamma < 1.7$; dark blue) and soft spectra ($\Gamma \geq 1.7$; light blue). Green: Comptonization models with unconstrained T_e (Fig. 2b). Red: model p -test < 0.05 fits. (Fig. 2c).

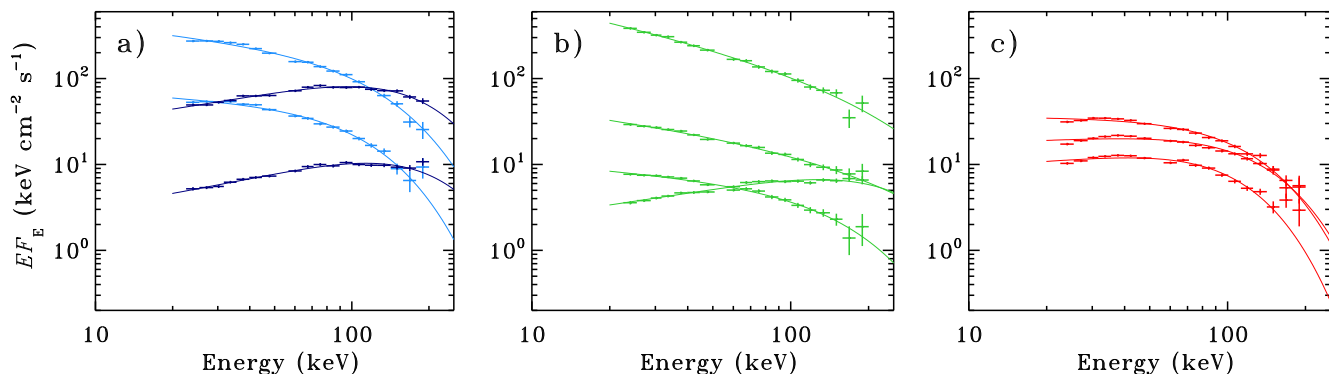


Fig. 2. Example of the spectra analyzed in this work. **Panel a)** Comptonized spectra displaying a cutoff at high energies within the IBIS/ISGRI energy range. We classify these spectra in two groups: *hard* ($\Gamma \leq 1.7$; dark blue) and *soft* ($\Gamma > 1.7$; light blue). The hardness selection is based on the Γ values derived using the *NTHCOMP* model. **Panel b)** Comptonized spectra for which T_e cannot be constrained by our data. We fixed the electron temperature to the value $T_e = 999$ keV in these spectral fits. Note the range in fluxes and hardness presented by these spectra. **Panel c)** spectra for which a Comptonized model was not statistically favored by our model selection criteria (p -test < 0.05). These spectra are predominantly found during the X-ray plateaus detected at fluxes $F_x \sim 5 \times 10^{-8} \text{ erg cm}^{-2} \text{ s}^{-1}$, as explained in the text.

model, and n is the number of channels in the spectral fits. In a model selection process, the optimal model is identified by the minimum value of BIC. A lower BIC implies either fewer explanatory variables, a better fit, or both. Kass (1995) set the strength of the evidence against the model with the higher BIC to be strong if $\Delta\text{BIC} > 6$, which we adopted as the limit for model selection. This approach was applied to the *NTHCOMP* and *COMPXS* fits. The results of this analysis are described in the following sections, and displayed in figures 1–8. In these figures the data are presented according to the following color convention:

- Blue points are used to highlight those fits where the ΔBIC model selection favored a Comptonization model with a constrained electron temperature T_e , further divided in two groups: ‘hard spectra’ ($\Gamma < 1.7$; dark blue) and ‘soft spectra’ ($\Gamma > 1.7$; light blue). Some of these spectra are shown in Fig. 2a. The latter classification is based on the Γ values derived from the *NTHCOMP* fits, and then applied to the *COMPXS* fits.

- Green points correspond to those spectra where T_e could not be constrained by our data (i.e. T_e fixed at 999 keV). Some of these spectra are shown in Fig. 2b.

- Additionally, for each fit we computed the corresponding p -value of the fit with respect to the data. We mark the spectra where $p < 0.05$ with red symbols. Some of these spectra are shown in Fig. 2c.

3. Results

3.1. Parameter evolution

We present in Fig. 1 the time evolution of the source flux computed in the 20–200 keV energy range, together with the evolution of the spectral parameters derived using *NTHCOMP* (Γ , T_e) and *COMPXS* (τ , T_e). Hereafter we will refer to the flux in the 20–200 keV energy range as F_x .

3.1.1. EPOCH 1: Flaring activity

During the period MJD 57191–57193 (Rev. 1554; EPOCH 1 in Fig. 1a) intense flaring activity was detected on timescales of minutes to hours. The flares reached peak fluxes of $F_x \sim 55 \times 10^{-8} \text{ erg cm}^{-2} \text{ s}^{-1}$. Between flares, we measure fluxes below $F_x \sim 2 \times 10^{-8} \text{ erg cm}^{-2} \text{ s}^{-1}$. Over this period, the IBIS/ISGRI spectrum was hard ($\Gamma \leq 1.7$), and only softened when F_x in-

creased above $\gtrsim 25 \times 10^{-8} \text{ erg cm}^{-2} \text{ s}^{-1}$ (i.e. during the peaks of the flares). T_e is well constrained during the X-ray flares, with values in the range 30–100 keV (*NTHCOMP*) or 30–70 keV (*COMPXS*). Between flares T_e cannot be constrained in our spectral fits, and the X-ray spectrum is consistent with a hard $\Gamma \leq 1.7$ power-law (see Fig. 2b). Similar results were obtained by Natalucci et al. (2015), who analyzed this data set using a different time resolution, and Roques et al. (2015), who analyzed contemporaneous *INTEGRAL*/SPI data.

In EPOCH 1 τ varies between 2 and 5. It displays higher values ($\tau \gtrsim 3.5$) when the spectrum is hard ($\Gamma \leq 1.7$), and decreases ($\tau \lesssim 3.5$) as the spectrum softens ($\Gamma > 1.7$; see Fig. 1d).

3.1.2. EPOCH 2: Spectral softening, state transitions, and X-ray plateaus

During the intervals MJD 57193.5–57195.5 and MJD 57196.7–57197.4 (Rev. 1555–1556; EPOCH 2 in figure 1a) the flaring activity persists, with peak fluxes of $F_p \sim 60\text{--}80 \times 10^{-8} \text{ erg cm}^{-2} \text{ s}^{-1}$. Between flares, we measure again fluxes $F_x \lesssim 2 \times 10^{-8} \text{ erg cm}^{-2} \text{ s}^{-1}$. In general, in EPOCH 2 the source tends to display softer spectra than during EPOCH 1 even at the lowest count rates, when $\Gamma \sim 2.3$ spectra with no cut-off are observed. Several transitions between Comptonized hard ($\Gamma \lesssim 1.7$) and soft ($\Gamma \sim 3$) spectra with unconstrained T_e are observed. Only one of the X-ray flares (detected around MJD 57195.15) displayed a hard X-ray spectrum ($\Gamma \leq 1.7$).

In this epoch, we observe more scatter in the measured T_e , τ and Γ parameters than in EPOCH 1. Also, the relation between F_x and Γ is complex: while during some flares Γ appears to be roughly constant (e.g. flare on MJD 57194.10, Fig. A.1), in other flares the spectrum hardens (e.g. flare on MJD 57195.5) or softens during the entire flare (e.g. flare on MJD 57194.3, Fig. A.1). During the flares, T_e displays values in the range 30–120 keV (*NTHCOMP*) or 20–150 keV (*COMPXS*). Very soft spectra ($\Gamma \sim 3$) with unconstrained T_e are detected by the end of this epoch, when the flux dropped below $\sim 2 \times 10^{-8} \text{ erg cm}^{-2} \text{ s}^{-1}$.

One additional feature over this period is the detection of X-ray plateaus (i.e. non-varying flux periods) at intermediate fluxes ($F_x \sim 5 \times 10^{-8} \text{ erg cm}^{-2} \text{ s}^{-1}$) lasting a few hours, in between successive X-ray flares (red points in Fig. 1; see also Rodríguez et al. 2015). For a closer view of one of these plateaus see Fig. A.1. We consistently obtain fit p -values < 0.05

when modeling the plateau spectra using Comptonization models (NTHCOMP or COMPPS), which also provide systematically lower electron temperatures for these data points ($T_e \sim 30$ keV) than those derived in fits to contemporaneous flare spectra ($T_e \sim 50$ keV). Joint spectral fits to simultaneous *Swift*/XRT, *INTEGRAL*/JEMX and *INTEGRAL*/ISGRI data by Motta et al. (2016) during one of these plateaus, showed a high absorption ($N_H \approx 1.4 \times 10^{24} \text{ cm}^{-2}$) over a dominant reflection component. Adding an absorption component (TBABS; $N_H \gtrsim 10^{24} \text{ cm}^{-2}$) to the fits to the plateau spectra, we obtain $T_e \sim 50$ keV, in better agreement with the values derived during contemporaneous flares. The N_H values obtained in these fits are presented in Fig. 1f. We observed that the highest N_H values are obtained precisely during the X-ray plateaus. However, the lack of simultaneous data in the soft X-rays (i.e., below 20 keV) prevents us to properly constraining N_H throughout the outburst.

3.1.3. EPOCH 3: Major flares and onset of outburst decay

Between MJD 57199.05 and MJD 57200.10 we observed two major flares separated by a long X-ray plateau. The first flare (MJD 57199.05–57199.15; Fig. A.2) reached a peak flux $F_x \sim 55 \times 10^{-8} \text{ erg cm}^{-2} \text{ s}^{-1}$. During this flare, the spectrum was hard ($\Gamma \leq 1.7$), contrary to the softer flares detected in EPOCH 2. We measure roughly constant electron temperatures ($T_e \sim 50$ keV) and an optical depth τ in the range [4–5.5], which decreased as the flare proceeded. The flare was followed by an X-ray plateau, similar to those seen in EPOCH2, during which $F_x \sim 5 \times 10^{-8} \text{ erg cm}^{-2} \text{ s}^{-1}$ was measured (Fig. A.2). The plateau lasted ~ 0.15 day.

After the plateau, we detect a major X-ray flare (MJD 57199.50–57199.80; Fig. A.3) during which the source reached the highest fluxes measured during the 2015 outburst ($F_x \sim 80 \times 10^{-8} \text{ erg cm}^{-2} \text{ s}^{-1}$). The flare has two peaks, separated by a ~ 1 hour flux drop (from ~ 70 to $\sim 20 \times 10^{-8} \text{ erg cm}^{-2} \text{ s}^{-1}$ and back to $\sim 80 \times 10^{-8} \text{ erg cm}^{-2} \text{ s}^{-1}$). Over the flare rise and decay we find a Comptonized, soft, X-ray spectrum that softened as F_x increased, and hardened as F_x decreased. T_e also evolved in correlation with the flux variations, and reached values above ~ 130 keV (NTHCOMP) or ~ 90 keV (COMPPS) during the peak of the flare. In some occasions around the peak T_e is not constrained by our fits (NTHCOMP).

During the flare decay we find an abrupt drop in flux, (from ~ 45 to $\sim 15 \times 10^{-8} \text{ erg cm}^{-2} \text{ s}^{-1}$), which happens in less than half an hour. The drop in flux is accompanied by a transition to harder spectra, characterized by a roughly constant power-law index ($\Gamma < 1.5$), an increasing T_e and decreasing τ . After the transition, the flux decay continues at a roughly constant Γ .

As the flux approached quiescence values, the spectrum softened again, T_e was unconstrained and the optical depth, τ , decreased. This period corresponds to the two lowest flux spectra in Fig. 2b.

3.2. Parameter distributions

The distributions of the spectral parameters derived in this analysis are displayed in Fig. 3. Note that the integration times of the spectra are flux dependent, and consequently the parameter distributions are skewed towards higher fluxes, where the sampling is more frequent.

The F_x distribution is shown in Fig. 3a and 3d. We measure fluxes in the range $[0.01\text{--}80] \times 10^{-8} \text{ erg cm}^{-2} \text{ s}^{-1}$ with a peak in the distribution at $\sim 50 \times 10^{-8} \text{ erg cm}^{-2} \text{ s}^{-1}$. We do

not find hard Comptonized spectra ($\Gamma \leq 1.7$) when $F_x \gtrsim 50 \times 10^{-8} \text{ erg cm}^{-2} \text{ s}^{-1}$. We find soft Comptonized spectra ($\Gamma \gtrsim 1.7$) for fluxes in the range $[4\text{--}80] \times 10^{-8} \text{ erg cm}^{-2} \text{ s}^{-1}$. We predominantly find Comptonized spectra with unconstrained electron temperatures at the lowest and highest fluxes. Spectra not compatible with Comptonized models are predominant in the range of fluxes $[1.5\text{--}6] \times 10^{-8} \text{ erg cm}^{-2} \text{ s}^{-1}$, with a peak in the distribution at $5 \times 10^{-8} \text{ erg cm}^{-2} \text{ s}^{-1}$.

The photon index (Γ ; Fig. 3b) was derived using the NTHCOMP model. The distribution of Γ values is asymmetric, with a peak at $\Gamma \sim 1.7$ and a tail extending to $\Gamma \sim 3.0$. We measure Γ values in the range $[1.5\text{--}2.4]$ for the Comptonized spectra with constrained T_e . All the Comptonized spectra softer than $\Gamma \gtrsim 2.4$ display unconstrained T_e in our NTHCOMP fits. There are also a fraction of hard spectra ($\Gamma \sim 1.7$) with unconstrained T_e . The spectra detected during X-ray plateaus display Γ values in the range $[1.6\text{--}3.0]$, with a peak in the distribution at $\Gamma = 1.8$.

The optical depth of the Comptonizing plasma (τ ; Fig. 3e), derived using COMPPS shows a large scatter in values, which are in the range $[0.1\text{--}5.0]$. The hard and soft spectra have different τ distributions. For the hard spectra ($\Gamma \leq 1.7$) we derive τ values in the range $[3\text{--}5.5]$. For the softer spectra ($1.7 < \Gamma \leq 2.4$) we derive τ values in the range $[0.1\text{--}4.5]$.

The electron temperatures that we derive using the NTHCOMP and COMPPS models (Figs. 3c and 3f) display similar distributions, with a narrow peak at moderate temperatures (NTHCOMP: 45 keV; COMPPS: 35 keV) and a tail extending up to ~ 150 keV. However, the distribution of T_e derived using NTHCOMP is broader than the distribution of values obtained from the COMPPS fits. We find more spectra with unconstrained T_e using NTHCOMP than using COMPPS, probably due to the systematically lower T_e values derived using COMPPS. The electron temperatures derived for Comptonized hard ($\Gamma \leq 1.7$) and soft spectra ($\Gamma > 1.7$) have consistent values, but we note that the tail of the T_e distribution extends to higher energies for the soft Comptonized spectra than for the hard ones. The fits to the spectra obtained during X-ray plateaus provide broad T_e distributions. They peak at lower energies than those derived for the Comptonized spectra (~ 25 keV) and extend up to ~ 130 keV.

3.3. Parameter relations

The flux dependencies of the photon index and optical depth are presented in the $F_x - \Gamma$ and $F_x - \tau$ diagrams (Fig. 4a, 4d). We find that the hard spectra in our sample ($\Gamma \leq 1.7$) occupy a region in the $F_x - \Gamma$ diagram reminiscent of the hard state in the BHB Hardness-Intensity Diagram (HID; Homan et al. 2001; Belloni 2004; Fender et al. 2004; Dunn et al. 2010). In this region, which we will call hereafter the *hard branch*, the spectrum softens (from $\Gamma \approx 1.5$ to $\Gamma \approx 1.7$) while the flux increases, and the optical depth increases with increasing flux from $\tau \sim 3$ to $\tau \sim 5.5$ (Fig. 4d). The hard spectra also occupy defined regions in the $F_x - T_e$, $\Gamma - T_e$, and $\tau - T_e$ diagrams (Fig. 4b, 4c, 4e, 4f). In these *hard branch(es)*, T_e is anti-correlated with F_x (figure 4b, 4e). We also find that T_e is anti-correlated with Γ and τ (4c, 4f).

The soft ($\Gamma > 1.7$) spectra in our sample, detected during the brightest X-ray flares, occupy a distinct region in the $F_x - \Gamma$ diagram (Fig. 4a) which we will call hereafter the *soft flaring branch*. In the *soft flaring branch* the spectrum still softens as the flux increases (Fig. 4a) even though most of the parameter dependencies are reversed with respect to the *hard branch*. τ is seen to decrease with increasing flux (Fig. 4d); F_x and T_e are correlated (Fig. 4b, 4e) and the $\Gamma - T_e$ dependency is also reversed. In the $\tau - T_e$ diagram, we find a range of τ values ($\tau \approx [2.5\text{--}4]$) for

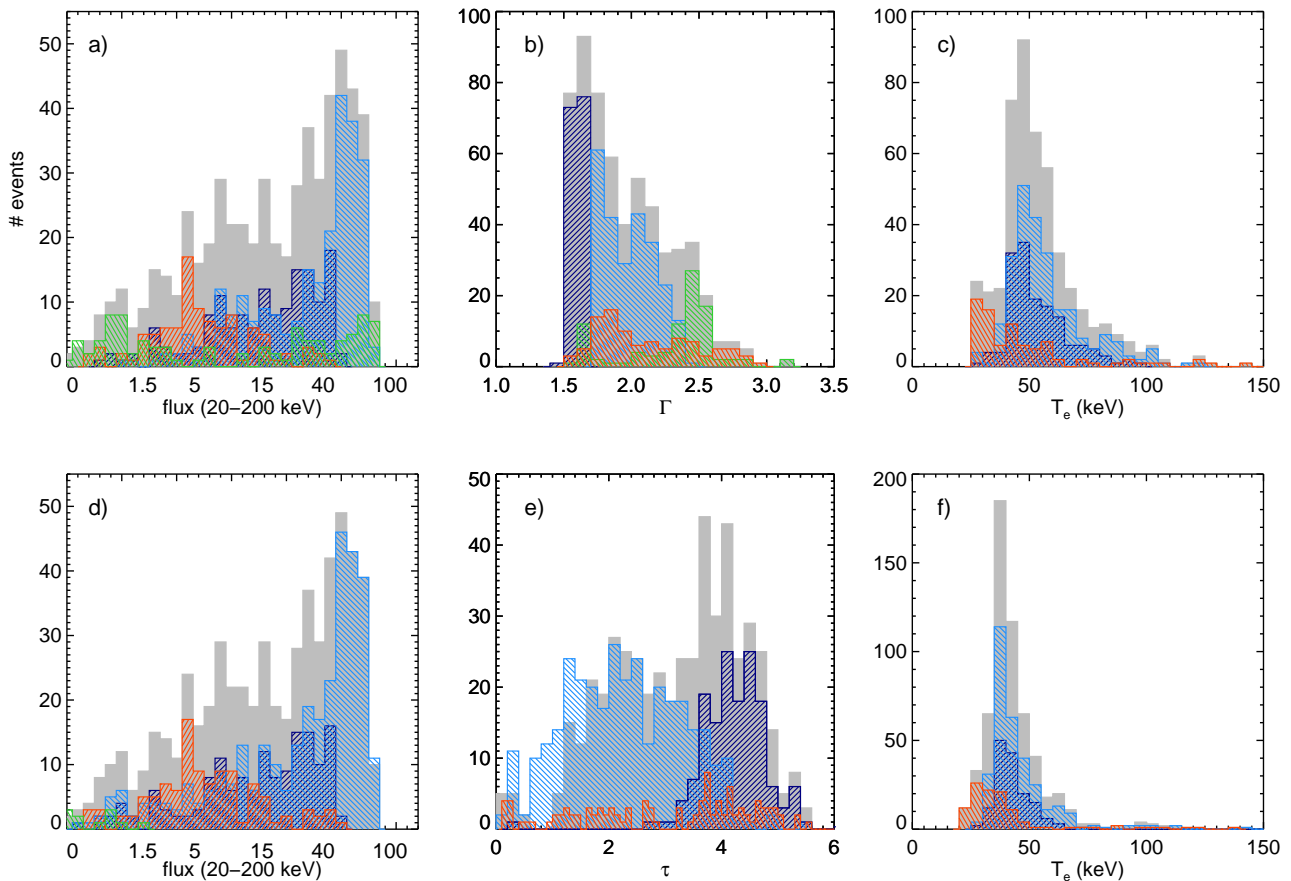


Fig. 3. Histograms displaying the distribution of the spectral parameters obtained in the fits to the IBIS/ISGRI spectra of V404 Cyg analyzed in this work. Grey bars are used to describe the total parameter distribution. Green, blue and red symbols are used to highlight the best-fitting model, according to our model selection criteria (Sect. 2.2). Blue: Comptonization models with constrained T_e (Fig. 2a) further divided into hard ($\Gamma < 1.7$; dark blue) and soft spectra ($\Gamma \geq 1.7$; light blue). Green: Comptonization models with unconstrained T_e (Fig. 2b). Red: p -test < 0.05 fits. (Fig. 2c). In the upper panels of the figure (a-c) we show the distribution of the N_{THCOMP} parameters, while in the lower panels we display the $COMPPS$ parameters.

which T_e displays a roughly constant value (~ 40 keV). Below $\tau \lesssim 2.5$, T_e and τ are anti-correlated (Fig. 4f).

For spectra softer than $\Gamma \gtrsim 2.4$ the spectra fits using N_{THCOMP} do not provide constrained electron temperatures. These soft spectra are detected at the highest ($\gtrsim 20 \times 10^{-8} \text{ erg cm}^{-2} \text{ s}^{-1}$) and lowest ($\lesssim 2 \times 10^{-8} \text{ erg cm}^{-2} \text{ s}^{-1}$) F_x values. When detected at the highest fluxes, they occupy regions in the $F_x - \Gamma$ diagram (Fig. 4a) reminiscent of the HID very high state (Dunn et al. 2010).

Finally, we also observe that the spectra detected during X-ray plateaus occupy separate regions in all these diagrams, distinct from the Comptonized branches, which confirms our classification of these spectra in a separate category. We will call these regions *plateau branch(es)*.

4. Discussion

The light curve of V404 Cyg during the June 2015 outburst does not display the typical features of the standard BHB light curves (e. g. Chen et al. 1997; Remillard & McClintock 2006). Similarly, the soft X-ray spectra of V404 Cyg is remarkably different from the spectra of other BHBs, mostly due to the extreme V404 Cyg intrinsic absorption (Motta et al. 2016), also seen in the 1989 outburst (Życki et al. 1999). However, when we look at the source spectra in hard X-rays (above 20 keV) where the ab-

sorption is not as important, we find some similarities between V404 Cyg and other BHBs.

4.1. Hard branch

We have identified a *hard branch* in the $F_x - \Gamma$ diagram, occupied by the hardest spectra in our sample ($\Gamma \lesssim 1.7$), which is reminiscent of the *hard state* in the HID (Homan et al. 2001; Belloni 2004; Fender et al. 2004; Dunn et al. 2010). When the source occupies the *hard branch*, the spectrum gradually softens and T_e decreases as the flux increases (Fig. 4a, 4d, 4b, 4e). This $F_x - T_e$ anti-correlation was observed during epoch 1 by Natalucci et al. (2015), Roques et al. (2015) and Jenke et al. (2016) using IBIS/ISGRI, SPI and *FERMI*/GBM data, respectively. Similar anti-correlations are found in other BHBs in the *hard state* (Esin et al. 1998; Wardziński et al. 2002; Rodriguez et al. 2003; Motta et al. 2009; Kajava et al. 2016), supporting our identification of the *hard branch* with the *hard state* of prototypical BHBs such as e.g. GX 339-4 (Belloni & Motta 2016). The $F_x - T_e$ anti-correlation can be explained in terms of the truncated disk/hot inner flow model (Esin et al. 1997; Mayer & Pringle 2007). At low luminosities the accretion disk is thought to be truncated far from the BH, so a small fraction of the disk photons reaches the hot flow/comptonizing medium. The X-ray spec-

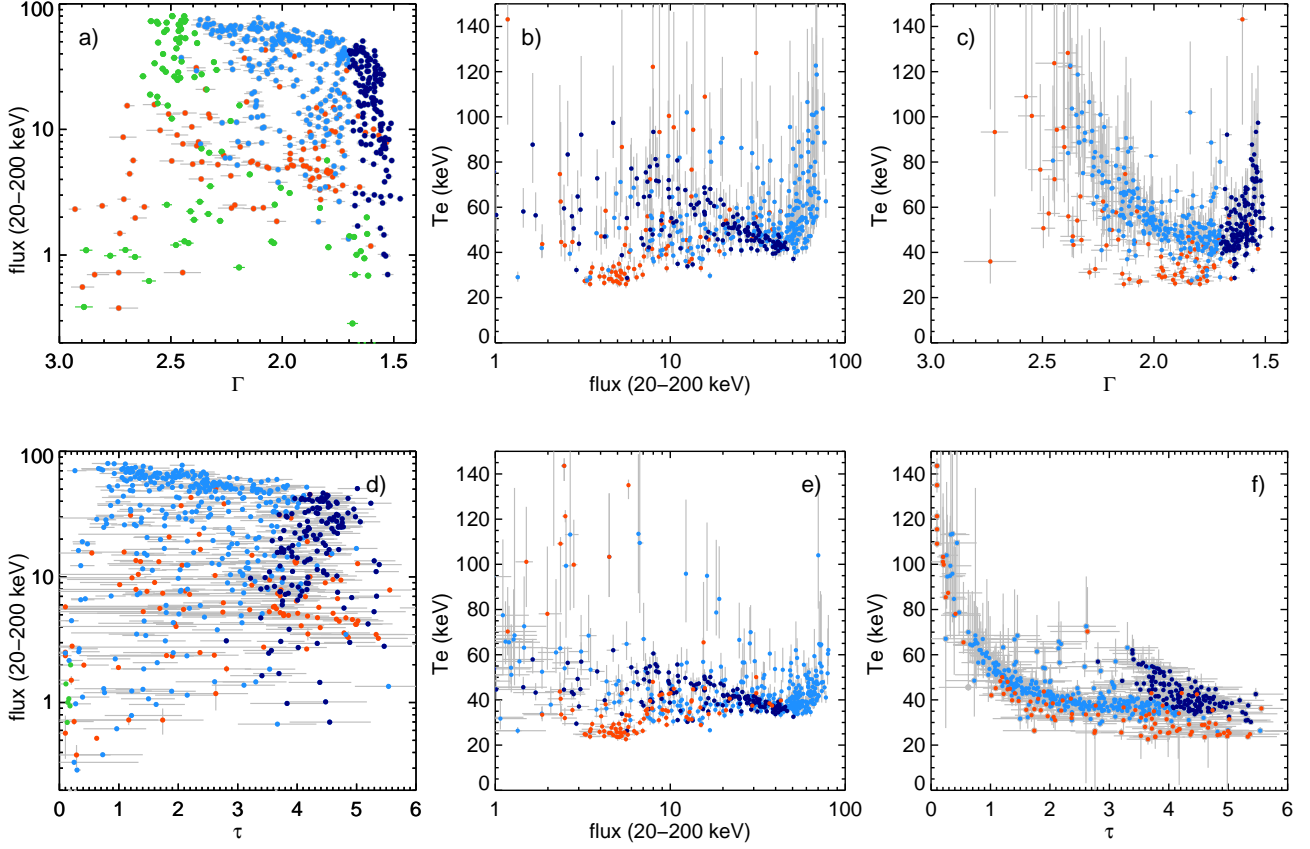


Fig. 4. Relations between the parameters derived from our spectral fits, using the NTHCOMP (panels a–c) and the COMPPS models (panels d–e). Green, blue and red symbols are used to highlight the best-fitting model, according to our model selection criteria (Sect. 2.2). Blue: Comptonization models with constrained T_e (Fig. 2a) further divided into hard ($\Gamma < 1.7$; dark blue) and soft spectra ($\Gamma \geq 1.7$; light blue). Green: Comptonization models with unconstrained T_e (Fig. 2b). Red: p -test < 0.05 fits. (Fig. 2c). **Panel a)** $F_x - \Gamma$ diagram. We find a *hard branch* (dark blue points) where F_x and Γ are anti-correlated, similar to the hard state in the BHB HID. We also find a *soft flaring branch* (light blue points), where the source exhibits the highest fluxes in the outburst, but the F_x and Γ anti-correlation persists. We identify the *soft flaring branch* with the BHB *intermediate states*. We also identify the softest spectra in our sample ($\Gamma \geq 2.4$) with unconstrained T_e with a tentative *very high state* (green points). **Panel d)** $F_x - \tau$ diagram. In the *hard branch* τ and F_x are correlated. In the *soft flaring branch* the relation reverses and τ and F_x are anti-correlated. **Panel b, e)** $F_x - T_e$ diagrams (NTHCOMP and COMPPS). In the *hard branch* F_x and T_e are anti-correlated. In the *soft flaring branch* F_x and T_e are correlated. **Panel c)** $\Gamma - T_e$ diagram. In the *hard branch* Γ and T_e are anti-correlated: softer spectra display cooler electron temperatures. In the *soft flaring branch* Γ and T_e are correlated: softer spectra display hotter electron temperatures, T_e becomes eventually unconstrained for $\Gamma > 2.4$. **Panel f)** $\tau - T_e$ diagram. In the *hard branch* τ and T_e are anti-correlated. In the *soft flaring branch* we observe a moderate anti-correlation between τ and T_e for τ in the range [2.5–5] and an anti-correlation between τ and T_e for $\tau < 2$, until T_e becomes eventually unconstrained as τ approaches zero.

trum is then modeled in terms of synchrotron self-Compton emission (SSC) in an hybrid (thermal plus non-thermal) Comptonizing medium (Poutanen & Vurm 2009; Malzac & Belmont 2009; Veledina et al. 2011). At fluxes below $\sim 10^{-8} \text{ erg cm}^{-2} \text{ s}^{-1}$, where we measure T_e in the range 60–80 keV (or unconstrained) V404 Cyg may be in this regime. As the accretion rate increases, the inner radius of the accretion disk moves inwards, closer to the BH. The result is that an increasing number of soft seed photons from the accretion disk enter the Comptonizing medium, gradually cooling down the population of thermal electrons to about $T_e \sim 40 \text{ keV}$. The electron cooling could cause the observed $F_x - T_e$ anti-correlation in the *hard branch*. It also results in softer Comptonized spectra (Done et al. 2007). Observations of GX 339–4 (Wardziński et al. 2002) and GRO J1655–40 (Joinet et al. 2008) in the *hard state* result in T_e values comparable to our measurements. However, these systems displayed lower τ values ($\tau \approx 2.5$), than those measured for V404 Cyg $\tau \approx [3–5.5]$, which means that we are dealing with an optically thick Comptonizing medium. These higher τ values are similar

to those found during the 1989 outburst of V404 Cyg ($\tau \approx 6$; Życki et al. 1999). As the optical depth is expected to scale linearly with the mass accretion rate (Różańska & Czerny 2000), the presence of an optically thick Comptonizing medium may be connected to V404 Cyg emitting closer to the Eddington limit than other BHBs in the *hard state*.

4.2. Soft flaring branch

In the *soft flaring branch* the spectrum still softens as the flux increases, but most of the parameter dependencies are reversed with respect to the *hard branch*, suggesting a change in the hard X-ray production mechanism: τ is anti-correlated with F_x (Fig. 4d); F_x and T_e are correlated (Fig. 4b, 4e) and the $\Gamma - T_e$ dependency is also reversed. These parameter correlations are similar to those observed during hard to soft state transitions in other BHBs (Philips et al. 1996; Esin et al. 1998; Joinet et al. 2008; Motta et al. 2009; Del Santo et al. 2013), suggesting that the *soft flaring branch* may correspond to the BHB *intermediate*

state. The observed decrease in τ is consistent with the material in the Comptonizing medium condensing into the disk, or being ejected during the transition (Malzac 2016). T_e increases as the flux progressively increases, suggesting that the injection of external (disk) photons, which cooled down the electron cloud in the *hard branch* might have ceased or its cooling effect on the electron cloud is negligible. Also, the detection of a cut-off in the spectrum is indicative of a significant fraction of thermal electrons. Both results are compatible with hard energy production via SSC emission (Ghisellini et al. 1988; Poutanen & Vurm 2009; Malzac & Belmont 2009; Veledina et al. 2011). In SSC models, T_e and τ are found to be anti-correlated (see Fig. 5 in Veledina et al. 2011).

The steepest spectra with $\Gamma \gtrsim 2.4$ (or $\tau \lesssim 1.0$) are the ones where T_e is not constrained (N_{THCOMP}). Fits to these data using `COMPBS` provide extremely low τ and high T_e values. At low optical depths the particles do not have time to cool between re-accelerations, and the electron distribution resembles the power-law injection function that could originate from magnetic re-connection or shock acceleration (Veledina et al. 2011; Del Santo et al. 2013). These spectra are detected at epochs bracketed by the largest measured T_e values ($\gtrsim 80$ keV), so it is likely that they are caused by the electron population becoming simultaneously hotter and/or progressively less thermal. When detected at the highest fluxes ($\gtrsim 20 \times 10^{-8} \text{ erg cm}^{-2} \text{ s}^{-1}$), the $\Gamma \gtrsim 2.4$ spectra occupy a region in the F_x - Γ diagram (Fig. 4a) reminiscent of the HID very high state (Dunn et al. 2010), which suggests that these spectra could be analogous to the very high state of GX 339-4 (Miyamoto et al. 1991; Kubota & Done 2016), GS 1124-68 (Miyamoto et al. 1993), XTE J1550-564 (Sobczak et al. 1999b; Kubota & Makishima 2004; Hjalmarsdotter et al. 2016), GRO J1655-40 (Sobczak et al. 1999a; Joinet et al. 2008), or 4U 1630-47 (Abe et al. 2005) where the spectrum is a composite of a strong disc and a steep prominent Comptonized tail, with no cutoff at high energies, which may extend up to ~ 1 MeV (Kubota & Done 2016).

When detected at the lowest fluxes, these $\Gamma \gtrsim 2.4$ spectra, could be analogous to the *soft state* spectra of some BHB where faint non-thermal hard X-ray tails are detected (Zdziarski et al. 2016).

4.3. X-ray plateaus

We have observed X-ray plateaus characterised by roughly constant fluxes ($F_x \sim 5 \times 10^{-8} \text{ erg cm}^{-2} \text{ s}^{-1}$) during periods lasting several hours. Often the plateaus are observed in between two or several flares (see Figs. 1, A.1). We have observed that the statistically worse fits tend to happen during these X-ray plateaus. Also, during the plateaus, the spectral parameters Γ and τ display values consistent with measurements during nearly contemporaneous flares, but T_e displays systematically lower values. Furthermore, we only detect X-ray plateaus in epoch 2 and 3, when the source is predominantly in the *soft flaring branch*, where the spectrum is softer. Spectral fits to simultaneous *Swift* and *INTEGRAL* data during the plateau detected around MJD 57194.2 (Fig. A.1) were performed by Motta et al. (2016), who found a heavily absorbed Comptonized spectrum ($N_H \approx 1.4 \times 10^{24} \text{ cm}^{-2}$) with a prominent reflection component. We also obtain very high N_H values ($N_H \sim 7 \times 10^{24} \text{ cm}^{-2}$; see Fig. 1f) when we add an absorption component (tbabs) to the fits to the plateau spectra and T_e values comparable to ~ 50 keV. Extreme N_H values can distort the IBIS/ISGRI spectrum at low energies and result in artificially lower T_e values when using Comptonization models (see

Fig. 2c). Our tests indeed indicate that these spectral fits are improved by adding variable ($N_H \gtrsim 10^{24} \text{ cm}^{-2}$) absorption. However, the energy range provided by IBIS/ISGRI results in large uncertainties in the N_H determination. Note also that Życki et al. (1999) measured measured N_H variability on timescales of minutes during the 1989 outburst. Therefore, it is likely that the dramatic intensity drops observed during these plateaus are caused by extreme by absorption/obscuration of the central source by some outflowing material, or by the outer regions of a Compton thick accretion disk, or by a combination of both. In these cases, most of the emission would be suppressed, and only the emission reflected by the obscuring material would reach the observer. This suggests, also, that the observed flaring activity may be partially caused by the Compton-thick obscuring material becoming occasionally Compton-thin and allowing the source photons to reach us. The fast flare rise and decay times (≈ 30 min, see Fig. A.1) may actually be related to varying partial obscuration of the central source, as previously suggested by Życki et al. (1999). Perhaps also for the same reason we find a lot of scatter in the correlations between F_x and the source spectral parameters (Γ, τ, T_e), while there is much less scatter in the various parameter correlations (Γ - T_e , τ - T_e see Fig. 4).

5. Summary of results and conclusions

We have fit the 20–200 keV IBIS/ISGRI spectra of V404 Cyg during the June 2015 outburst using two thermal Comptonization models (N_{THCOMP} and `COMPBS`). For the first time we have continuously measured the evolution of the properties of the Comptonizing medium during an outburst rise and decay. We find that the system evolves through the same Γ - T_e , τ - T_e and F_x - T_e paths during the outburst rise and decay. We have identified two clear spectral branches in the F_x - Γ diagram which display characteristic parameter relations: a *hard branch* and a *soft flaring branch*.

In the *hard branch*, V404 Cyg shows a hard ($\Gamma \leq 1.7$) thermal Comptonized spectrum, which slowly softens as the flux increases. In the *hard branch*, τ is correlated with the F_x while T_e is anti-correlated with F_x and Γ . Similar parameter correlations have been observed in other BHBs in the *hard state*, suggesting that the *hard branch* could correspond to the HID *hard state*. The observed parameter evolution can be explained in terms of thermal Comptonization of soft seed photons by a hot electron cloud in the vicinity of the BH. The F_x T_e anti-correlation could result from the electron population progressively cooling down as the accretion disk moves closer to the BH and more disk photons enter the Comptonizing medium.

In the *soft flaring branch* V404 Cyg shows a soft, thermal Comptonized spectrum, ($\Gamma > 1.7$), which gradually softens as the flux increases. In the *soft flaring branch* T_e and F_x are correlated, while F_x and τ are anti-correlated. The parameter correlations are consistent with those observed during *hard* to *soft* state transitions in other sources, suggesting that these data could correspond to the *intermediate state* or occasionally the *very high state*. The observed T_e - F_x correlation is compatible with the predictions of SSC-models.

We have also found a *plateau branch* where Comptonization models fail to describe the source spectra likely because of extreme absorption (even at energies $\gtrsim 20$ keV). This absorption can be produced by some outflowing material obscuring the central source. We propose that the observed dramatic flaring activity seen at hard X-rays may not only be due intrinsic source variability, but can partly result from obscuration of the central source. In the most extreme cases (e.g. during X-ray plateaus) the emission observed in the IBIS/ISGRI energy range may just

be the contribution of X-rays reflected off the absorbing material. The system inclination of 67° may be a key parameter in generating such a rich phenomenology, not observed in other sources observed at lower or higher inclination angles.

Acknowledgements. JJEK acknowledges support from the ESA research fellowship programme. SEM acknowledges support from the Faculty of the European Space Astronomy Centre (ESAC).

References

- Abe, Y., Fukazawa, Y., Kubota, A., Kasama, D., & Makishima, K. 2005, *PASJ*, 57, 629
- Barthelmy, S. D. & Sbarufatti, B. 2015, *GRB Coordinates Network*, 17963
- Belloni, T. 2004, *Nuclear Physics B Proceedings Supplements*, 132, 337
- Belloni, T. M. & Motta, S. E. 2016, in *Astrophysics and Space Science Library*, Vol. 440, *Astrophysics of Black Holes: From Fundamental Aspects to Latest Developments*, ed. C. Bambi, 61
- Beloborodov, A. M. 1999, in *ASP Conf. Ser. 161: High Energy Processes in Accreting Black Holes*, ed. J. Poutanen & R. Svensson, 295
- Casares, J., Charles, P. A., & Naylor, T. 1992, *Nature*, 355, 614
- Chen, W., Shrader, C. R., & Livio, M. 1997, *ApJ*, 491, 312
- Courvoisier, T. J.-L., Walter, R., Beckmann, V., et al. 2003, *A&A*, 411, L53
- Del Santo, M., Malzac, J., Belmont, R., Bouchet, L., & De Cesare, G. 2013, *MNRAS*, 430, 209
- Done, C., Gierliński, M., & Kubota, A. 2007, *A&A Rev.*, 15, 1
- Droulans, R., Belmont, R., Malzac, J., & Jourdain, E. 2010, *ApJ*, 717, 1022
- Dunn, R. J. H., Fender, R. P., Körding, E. G., Belloni, T., & Cabanac, C. 2010, *MNRAS*, 403, 61
- Ebisawa, K., Ogawa, M., Aoki, T., et al. 1994, *PASJ*, 46, 375
- Eikenberry, S. S., Dallilar, Y., Garner, A., et al. 2016, in *AAS/High Energy Astrophysics Division*, Vol. 15, *AAS/High Energy Astrophysics Division*, 109.01
- Esin, A. A., McClintock, J. E., & Narayan, R. 1997, *ApJ*, 489, 865
- Esin, A. A., Narayan, R., Cui, W., Grove, J. E., & Zhang, S.-N. 1998, *ApJ*, 505, 854
- Fender, R. P., Belloni, T. M., & Gallo, E. 2004, *MNRAS*, 355, 1105
- Ferrigno, C., Bozzo, E., Boissay, R., Kuulkers, E., & Kretschmar, P. 2015, *The Astronomer's Telegram*, 7731
- Gandhi, P., Littlefair, S. P., Hardy, L. K., et al. 2016, *MNRAS*, 459, 554
- Ghisellini, G., Guilbert, P. W., & Svensson, R. 1988, *ApJ*, 334, L5
- Gierliński, M., Zdziarski, A. A., Poutanen, J., et al. 1999, *MNRAS*, 309, 496
- Hjalmarsdotter, L., Axelsson, M., & Done, C. 2016, *MNRAS*, 456, 4354
- Homan, J., Wijnands, R., van der Klis, M., et al. 2001, *ApJS*, 132, 377
- Jenke, P. A., Wilson-Hodge, C. A., Homan, J., et al. 2016, *ApJ*, 826, 37
- Joinet, A., Jourdain, E., Malzac, J., et al. 2007, *ApJ*, 657, 400
- Joinet, A., Kalemci, E., & Senziani, F. 2008, *ApJ*, 679, 655
- Kajava, J. J. E., Veledina, A., Tsygankov, S., & Neustroev, V. 2016, *A&A*, 591, A66
- Kass, R., Raftery, A. 1995, *Journal of the American Statistical Association*, 90, 773
- Khargharia, J., Froning, C. S., & Robinson, E. L. 2010, *ApJ*, 716, 1105
- Kimura, M., Isogai, K., Kato, T., et al. 2016, *Nature*, 529, 54
- Kubota, A. & Done, C. 2016, *MNRAS*, 458, 4238
- Kubota, A. & Makishima, K. 2004, *ApJ*, 601, 428
- Kuulkers, E. 2015, *The Astronomer's Telegram*, 7758
- Lebrun, F., Leray, J. P., Lavocat, P., et al. 2003, *A&A*, 411, L141
- Loh, A., Corbel, S., Dubus, G., et al. 2016, *MNRAS*, 462, L111
- Makino, F. 1989, *IAU Circ.*, 4782
- Malzac, J. 2016, *Astronomische Nachrichten*, 337, 391
- Malzac, J. & Belmont, R. 2009, *MNRAS*, 392, 570
- Malzac, J., Petrucci, P. O., Jourdain, E., et al. 2006, *A&A*, 448, 1125
- Marsden, B. G. 1989, *IAU Circ.*, 4783
- Mayer, M. & Pringle, J. E. 2007, *MNRAS*, 376, 435
- McConnell, M. L., Zdziarski, A. A., Bennett, K., et al. 2002, *ApJ*, 572, 984
- Miller-Jones, J. C. A., Jonker, P. G., Dhawan, V., et al. 2009, *ApJ*, 706, L230
- Miyamoto, S., Iga, S., Kitamoto, S., & Kamado, Y. 1993, *ApJ*, 403, L39
- Miyamoto, S., Kimura, K., Kitamoto, S., Dotani, T., & Ebisawa, K. 1991, *ApJ*, 383, 784
- Motta, S., Belloni, T., & Homan, J. 2009, *MNRAS*, 400, 1603
- Motta, S., Homan, J., Muñoz Darias, T., et al. 2012, *MNRAS*, 427, 595
- Motta, S. E., Kajava, J. J. E., Sánchez-Fernández, C., Giustini, M., & Kuulkers, E. 2016, *ArXiv e-prints [arXiv:1607.02255]*
- Muñoz-Darias, T., Casares, J., Mata Sánchez, D., et al. 2016, *Nature*, 534, 75
- Narayan, R. & Yi, I. 1995, *ApJ*, 452, 710
- Natalucci, L., Fiocchi, M., Bazzano, A., et al. 2015, *ApJ*, 813, L21
- Negoro, H., Matsumitsu, T., Mihara, T., et al. 2015, *The Astronomer's Telegram*, 7646
- Oosterbroek, T., van der Klis, M., Vaughan, B., et al. 1996, *A&A*, 309, 781
- Phlips, B. F., Jung, G. V., Leising, M. D., et al. 1996, *ApJ*, 465, 907
- Poutanen, J. & Svensson, R. 1996, *ApJ*, 470, 249
- Poutanen, J. & Veledina, A. 2014, *Space Sci. Rev.*, 183, 61
- Poutanen, J. & Vurm, I. 2009, *ApJ*, 690, L97
- Remillard, R. A. & McClintock, J. E. 2006, *ARA&A*, 44, 49
- Richter, G. A. 1989, *Information Bulletin on Variable Stars*, 3362
- Rodriguez, J., Cadolle Bel, M., Alfonso-Garzón, J., et al. 2015, *A&A*, 581, L9
- Rodriguez, J., Corbel, S., & Tomsick, J. A. 2003, *ApJ*, 595, 1032
- Roques, J.-P., Jourdain, E., Bazzano, A., et al. 2015, *ApJ*, 813, L22
- Różańska, A. & Czerny, B. 2000, *A&A*, 360, 1170
- Schwarz, G. 1978, *Annals of statistics*, 6, 461
- Segreto, A., Del Santo, M., D'Ai, A., et al. 2015, *The Astronomer's Telegram*, 7755
- Shakura, N. I. & Sunyaev, R. A. 1973, *A&A*, 24, 337
- Shapiro, S. L., Lightman, A. P., & Eardley, D. M. 1976, *ApJ*, 204, 187
- Siebert, T., Diehl, R., Greiner, J., et al. 2016, *Nature*, 531, 341
- Sivakoff, G. R., Bahramian, A., Altamirano, D., et al. 2015, *The Astronomer's Telegram*, 7959
- Sobczak, G. J., McClintock, J. E., Remillard, R. A., Bailyn, C. D., & Orosz, J. A. 1999a, *ApJ*, 520, 776
- Sobczak, G. J., McClintock, J. E., Remillard, R. A., et al. 1999b, *ApJ*, 517, L121
- Sunyaev, R. A. & Truemper, J. 1979, *Nature*, 279, 506
- Tanaka, Y. 1989, in *ESA Special Publication*, Vol. 296, *Two Topics in X-Ray Astronomy*, Volume 1: X Ray Binaries. Volume 2: AGN and the X Ray Background, ed. J. Hunt & B. Batrick
- Tetarenko, A., Sivakoff, G. R., Young, K., Wouterloot, J. G. A., & Miller-Jones, J. C. 2015, *The Astronomer's Telegram*, 7708
- Veledina, A., Vurm, I., & Poutanen, J. 2011, *MNRAS*, 414, 3330
- Walton, D., Harrison, F., Forster, K., et al. 2015, *The Astronomer's Telegram*, 7752
- Walton, D. e. 2016, in *AAS/High Energy Astrophysics Division*, Vol. 15, *AAS/High Energy Astrophysics Division*, 109.08
- Wardziński, G., Zdziarski, A. A., Gierliński, M., et al. 2002, *MNRAS*, 337, 829
- Winkler, C., Courvoisier, T. J.-L., Di Cocco, G., et al. 2003, *A&A*, 411, L1
- Younes, G. 2015, *GRB Coordinates Network*, 17932
- Zdziarski, A. A., Johnson, W. N., & Magdziarz, P. 1996, *MNRAS*, 283, 193
- Zdziarski, A. A., Lubiński, P., & Sikora, M. 2012, *MNRAS*, 423, 663
- Zdziarski, A. A., Malyshev, D., Chernyakova, M., & Pooley, G. G. 2016, *ArXiv e-prints [arXiv:1607.05059]*
- Życki, P. T., Done, C., & Smith, D. A. 1999, *MNRAS*, 309, 561

Appendix A: Closer view to some flares

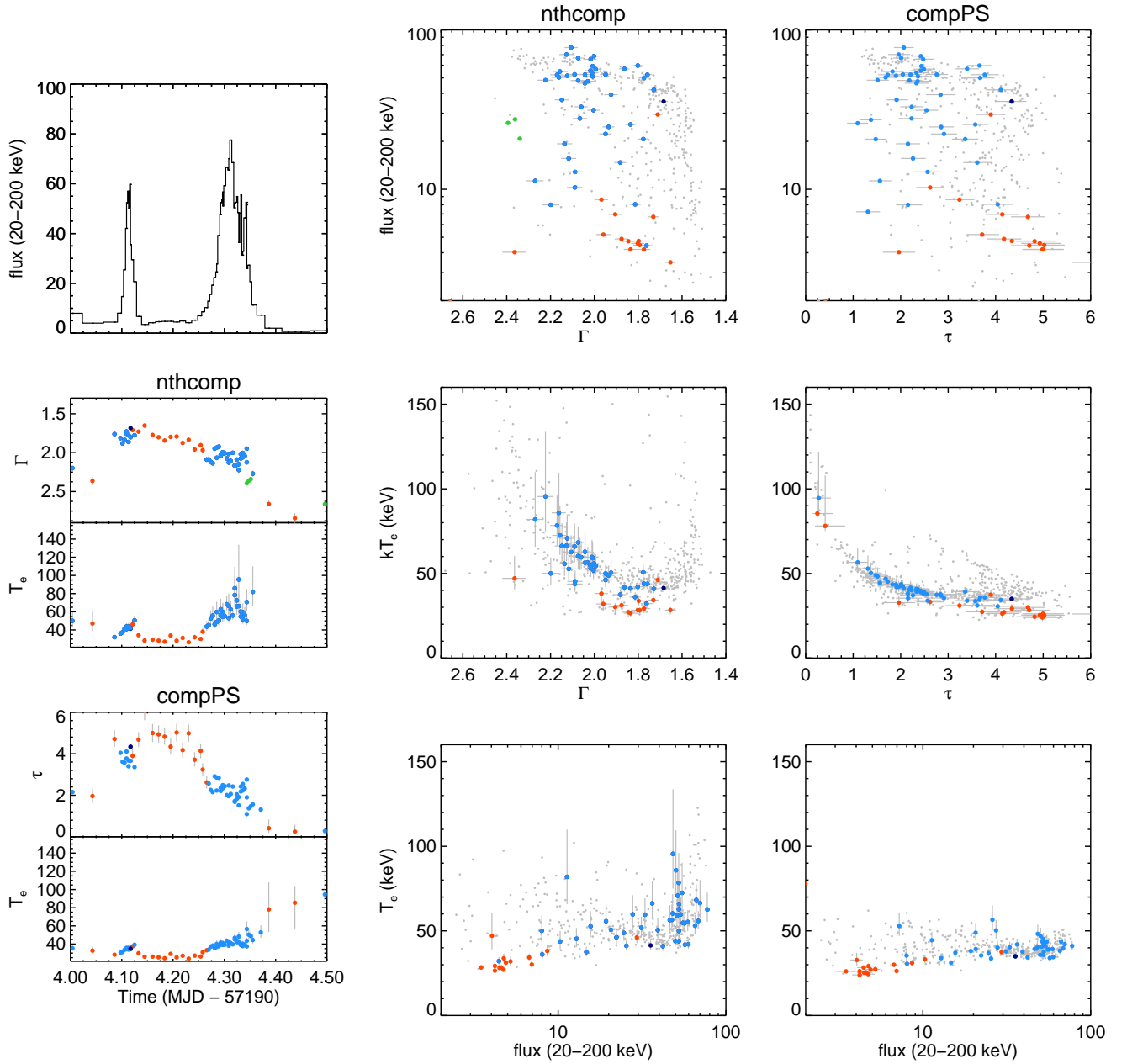


Fig. A.1. Close view to the properties of the X-ray plateau detected on MJD 57194. The plots in the left column provide the time evolution of the system flux and spectral parameters during this time interval, as derived using Comptonization models (*nthcomp* and *compPS*). The plots in the center and right side of the figure describe the relations between these spectral parameters derived using *nthcomp* (middle panel) and *compPS* (right panel). The plateau is characterised by a roughly constant flux, F_x interrupted by two major X-ray flares with peak count rates of $F_x \sim 60$ and $80 \times 10^{-8} \text{ erg cm}^{-2} \text{ s}^{-1}$. The Γ and τ parameters derived during the plateau display values consistent with the trend observed during the flares, while the electron temperatures are systematically lower values than measured in the flare spectra. Fits to the plateau spectrum around MJD 57194.2 by Motta et al. (2016) show that it is consistent with a heavily absorbed ($N_H \approx 1.4 \times 10^{24} \text{ cm}^{-2}$) Comptonization spectrum, with a prominent reflection component, likely the result of an almost complete obscuration of the inner accretion flow by a geometrically thick accretion flow. Extreme N_H values can distort the IBIS/ISGRI spectrum at low energies, artificially reducing T_e when using pure Comptonization models (see Fig. 2c). The parameters derived during the peaks of the flares occupy the *soft flaring branch*, and display typical spectral characteristics of this region (see Sect. 3.3), while the flare rise and decays, still very likely affected by obscuration, occupy intermediate regions between the *soft flaring branch* and the *plateau branch* in the Γ – T_e , τ – T_e and F_x – T_e diagrams.

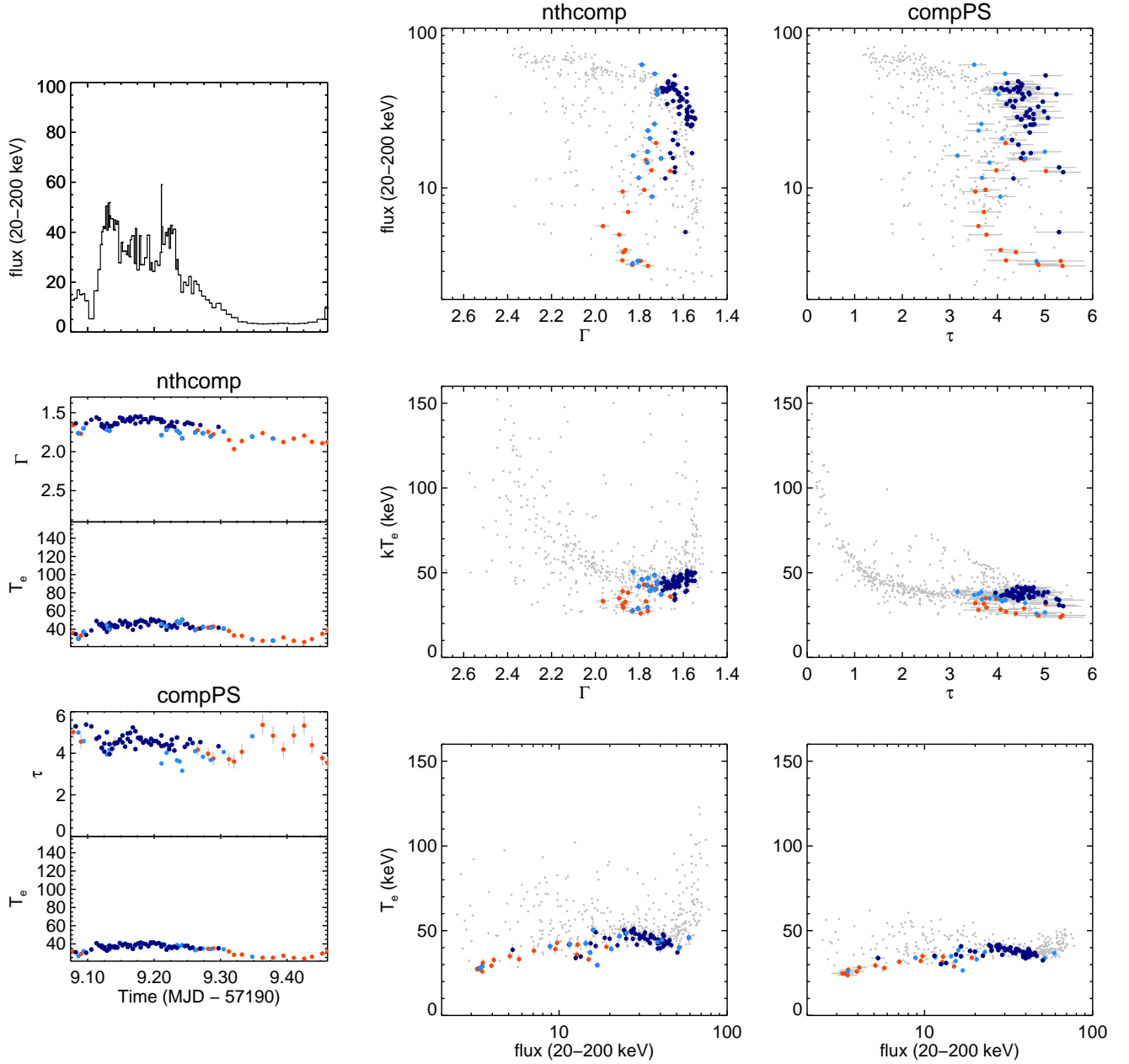


Fig. A.2. Close view to the properties of the hard X-ray flare detected around MJD 55199. The flare is followed by an X-ray plateau also shown in the figure. The plots in the left column provide the time evolution of the system flux and spectral parameters during this time interval, as derived using Comptonization models (*nthcomp* and *compPS*). The plots in the center and right side of the figure describe the relations between these spectral parameters derived using *nthcomp* (middle panel) and *compPS* (right panel). The flare displays dramatic changes in flux, accompanied by little variations in Γ and τ . It occupies the brightest F_x regions of the *hard branch* (see Sect. 3.3) in the F_x - Γ , F_x - τ and F_x - T_e diagrams, where T_e is anti-correlated with F_x and τ . Some, brief transitions to the *soft flaring branch* are observed during the peak of the flare. Following the peak, F_x gradually drops to an X-ray plateau, the spectrum gradually softens, T_e decreases and τ displays high variability. The various parameter correlations reverse in the *plateau branch* with respect to the trends observed in the *hard branch*, which otherwise displays typical *soft flaring branch* values, but at lower fluxes.

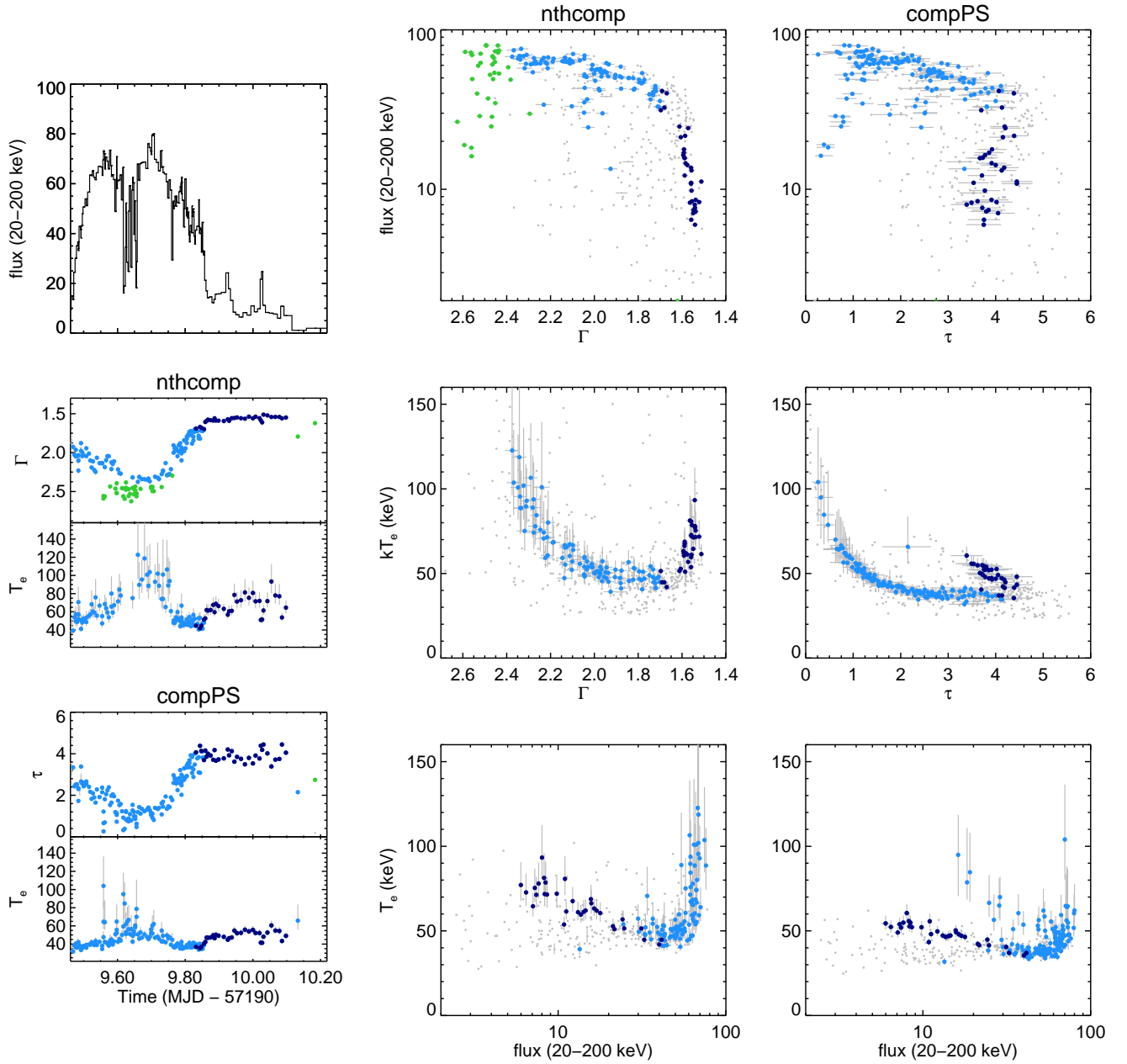


Fig. A.3. Close view to the properties of the major X-ray flare detected around MJD 57200. The plots in the left column provide the time evolution of the system flux and spectral parameters derived using Comptonized models (NTHCOMP and COMPPS). The plots in the center and right side of the figure describe the relations between the different spectral parameters measured during this time interval using NTHCOMP (middle panel) and COMPPS (right panel). During rise and decay, the flare displays parameter correlations characteristic of the *soft flaring branch*: Γ and τ are anti-correlated with F_x while T_e is correlated with F_x . Around the peak of the flare, the spectra soften above $\Gamma \sim 2.4$ and T_e cannot be constrained using NTHCOMP. Spectral fits to these data using COMPPS provide (constrained) high T_e values ($T_e \gtrsim 100$ keV), and the lowest τ values found in this work ($\tau \lesssim 1$). These spectra occupy a region in the Γ – F_x diagram reminiscent of the BH *very high state*. They also occupy a separate branch in the COMPPS F_x – T_e diagram. After the flare peak, as F_x decreased, and the spectrum hardened below $\Gamma \sim 2.4$ the system returned to the *soft flaring branch*, and F_x started to decrease from the peak values. Around MJD 57199.85, when the system entered the *hard branch* a dramatic drop in flux F_x was observed (from ~ 50 to $\sim 15 \times 10^{-8}$ erg cm $^{-2}$ s $^{-1}$ in about half an hour), as the system entered the *hard branch*. After this transition, the system started the decay to quiescence, displaying the characteristic *hard branch* correlations observed during the flare rise, but for a decreasing flux: the optical depth decreased and the spectrum gradually hardened as the flux decayed, while the electrons were seen to gradually heat up.